Journal of Advanced Ceramics
2019, **8**(4): 500–508
https://doi.org/10.1007/s40145-019-0330-8
ISSN 2226-4108
CN 10-1154/TQ

Research Article

Unveiling the reaction products in heat treated Si_3N_4–Ti joined ceramics by transmission electron microscopy

Orkun TUNCKAN[a], Hilmi YURDAKUL[b], Servet TURAN[c,*]

[a]*Faculty of Aeronautics and Astronautics*, *Eskisehir Technical University*, *Eskisehir 26480*, *Turkey*
[b]*Rafet Kayis Faculty of Engineering*, *Department of Metallurgical and Materials Engineering*, *Alanya Alaaddin Keykubat University*, *Alanya-Antalya 07450*, *Turkey*
[c]*Faculty of Engineering*, *Department of Materials Science and Engineering*, *Eskisehir Technical University*, *Eskisehir 26480*, *Turkey*

Received: December 21, 2018; Revised: March 21, 2019; Accepted: April 8, 2019

Abstract: Joining is a crucial process for the production of complex-shaped advanced engineering materials. Deep understanding of ceramic–metal interfaces during joining or following heat-treatment steps is therefore of important concern in designing the new systems. Capacitor discharge joining (CDJ) method was firstly carried out to compose the ceramic–metal joint material by silicon nitride (Si_3N_4)–titanium (Ti) constituents. Afterwards, heat treatment was performed on the Si_3N_4–Ti joints in air atmosphere at 1000 ℃ temperature to reveal the interface reactions and phases. Reaction layer that occurred between the Si_3N_4 and Ti interfaces and new phase formations were examined by transmission electron microscopy (TEM)-based various imaging and chemical analysis techniques. Electron transparent samples for TEM characterization were prepared by focused ion beam (FIB) milling and lifting method. Based on the detailed TEM results, Si and N diffusion arising from the Si_3N_4 ceramic was observed towards Ti metal foil side and further interacted with Ti atoms. The upshot of current diffusion was that Ti_3N_2 reaction layer with 50 nm thickness was formed at the interface while titanium silicon nitride (Ti_6Si_3N) matrix phase including dendritic-shaped Ti_2N grains occurred in the Ti interlayer. It is believed that our TEM-based microscopy results not only provide the knowledge on ceramic–metal joint materials by CDJ method, but also contribute new insights on the development of various new joint systems.

Keywords: capacitor discharge joining (CDJ); Si_3N_4; Ti; transmission electron microscopy (TEM)

1 Introduction

Silicon nitride ceramics (Si_3N_4) are mostly used in high-temperature structure and wear-resistant components combined with metallic materials in many different areas, such as automotive, aircraft, aerospace, and electronic industries, and also used as cutting tools for machining application [1–3]. On the other hand, titanium (Ti) and its alloys have been crucial materials for aerospace, nuclear, and chemical industries for their excellent chemical properties [4–6]. Considering these advantages and practical needs for Si_3N_4 and Ti materials in industry, reliable joining techniques have

* Corresponding author.
E-mail: sturan@eskisehir.edu.tr

to be utilized since Si_3N_4 has some difficulty for machining and producing complex shape [7]. For instance, while Si_3N_4 ceramics have excellent thermal, oxidation, and creep resistance, metallic material can be used as an interlayer to compensate stress or temperature gradient of structures and moving parts [8]. However, some factors such as differences in thermal expansion coefficient between ceramic and metal, bonding time, and resulting reaction products can directly affect the mechanical properties of joints depending on the chosen technique parameters and properties of the filler materials [9,10].

Based on the joining type, to obtain desirable chemical and mechanical properties, different interlayer materials have been used for different ceramics. The most comprehensively utilized alloys as an interlayer in Si_3N_4-based ceramics are mostly combining with Cu, Ag, Ni, Nb, Ta, Zr, Hf, Pd, V, Fe, Co, and Ti. For instance, Ag–Cu eutectic alloys containing Ti have been used very widely so far since strong wetting, spreading, and bonding effects of active Ti metal on the ceramic surfaces can be achieved [11,12]. On the other hand, a number of studies have examined and calculated Si_3N_4–Ti, Ti–Si, Ti–N, and Ti–Si–N systems using different techniques such as diffusion bonding [13,14], ultrasonic brazing [15–17], *in situ* synthesis method [18], diffusion couples [19,20], and thermo-dynamic programs [21–23]. Especially, ultrasonic brazing technique has attracted significant attention recently, since it enables the bonding of dissimilar materials at low cost and in fast bonding time [15–17].

Nevertheless, especially main joining process techniques such as diffusion bonding, active metal brazing, and liquid phase bonding generally take long time, so it can alter the properties of the ceramic [24]. However, the capacitor discharge joining (CDJ) method [24–28] delivers a chance to investigate the preliminary reactions and phase formations. It is because CDJ is a very speedy technique and no necessity for a special atmosphere or heating.

The purpose and motivation of present research is mainly to apply a heat treatment process at 1000 ℃ in air atmosphere on a ceramic–metal joint material consisted of Si_3N_4–Ti phases through CDJ method. Afterwards, the occurrences and transformations of newly formed phases based on the applied heat treatment route are to reveal in the complete reaction mechanisms by using novel transmission electron microscopy (TEM)-based different imaging and analytical techniques.

2 Materials and methods

The schematic representation of the CDJ technique is shown in Fig. 1. In this CDJ method, the Ti foil was positioned between Si_3N_4 parts and connected to a capacitor with the copper (Cu) electrodes. After the charging of the capacitor to 7 kV, the stored electricity was suddenly discharged, and hence the energy was used to melt the foil. At the same time, the 1000 kg compressive pressure was approximately applied to the sandwiched sample. The joining was completed in few micro seconds [28].

To understand the nature of chemical reactions that can occur at the interfaces and to compare with the as-received samples which were produced in our previous study [25], heat treatment process was carried out at 1000 ℃. This temperature was selected since during the dry cutting process, temperature of ceramic cutting tool edge was roughly increased to 1000 ℃ due to friction. As a result of this heat affect, undesirable reaction products may occur so that these products can be examined with electron microscopy techniques via heat treatment to resemble machining.

To get accurate and precise results from TEM characterization, electron transparent samples were prepared by focused ion beam (FIB) milling and lifting method using the FEI-Nova NanoLab 600 DualBeam™ instrument. Herein, a special region from the interface in heat-treated sample was intentionally chosen. Then, a thin platinum (Pt) layer was coated onto this region to protect the specimen. Afterwards, ion milling was started to further thin the selected part of interface by gallium (Ga) ion bombardment for both faces of Pt layer. Following, a microprobe was used to lift out the sliced region and attached to Cu TEM grid for end milling part of process. Finally, the sample was ready to be examined by TEM analysis in dimensions of 10 μm length, 5 μm width, and 50 nm thickness.

TEM analyses were performed by a field emission gun (FEG) microscope (JEOL 2100F attached with Gatan

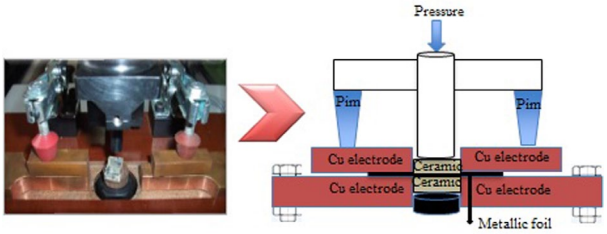

Fig. 1 Schematic representation of the capacitor discharge technique.

GIF Tridiem STEMPack energy filter and scanning (S)TEM detectors-bright field (BF), annular dark filed (ADF), and Fischione high angle annular dark field (HAADF) under the 200 kV accelerating voltage. Here, electron energy loss spectroscopy (EELS) in STEM mode, spectrum imaging (SI) in both STEM and energy filtering (EF) TEM mode, and EFTEM 3-window elemental mapping analyses were performed. In EELS analysis, 1–2 nm electron spot and 30–40 s acquisition time were chosen to acquire the high signal to noise ratio (S/N). Also, 9.2 and 15.7 mrad values were respectively determined for convergence and collection semi angles. Moreover, in EFTEM–SI and EELS–SI analyses, beam and image drift artifacts were controlled and removed by a corrector that plugged in Gatan DigitalMicrograph^{TM} software. 0.2 and 0.5 eV/ channels for energy filtering spectrometer dispersions were also selected to obtain high S/N. Background removal process for both acquired and reference EELS spectra were carried out based on the powerlaw.

3 Results

To determine exact chemical composition of reaction products and to further understand the elemental changing by heat-treatment in the Si_3N_4–Ti ceramic–metal joint material, TEM-based imaging and chemical characterizations were performed (Figs. 2–7). STEM–HAADF (Figs. 2(a), 2(c), and 2(e)), zero loss images of FIBed (Fig. 2(b)), and BF (Figs. 2(d)–2(f)) images of Si_3N_4–Ti joints were given for different magnification values in Fig. 2. Based on the atomic number (Z)–contrast–HAADF images, the effect of heat treatment was clearly seen within Ti interlayer and ceramic–metal interface (Figs. 2(c)–2(e)). Some of the white–grey contrast for dendritic-shaped phases and dark contrast with spherical phases that have fewer atomic numbers than Ti was seen at the interlayer. Also, reaction layer (RL) was detected in Si_3N_4–Ti interface with around 50 nm continuous thickness. Higher magnification of this RL (which is shown by rectangular in Figs. 2(c) and 2(d)) was given for both HAADF and BF techniques (Figs. 2(e) and 2(f)). Based on Z contrast STEM–HAADF image in Figs. 2(c)–2(e), some parts of the formations and dendrites show the variable contrast from white to grey due to Z differences of phases, whereas the same regions can be discerned in opposite contrast in STEM–BF image that was governed by

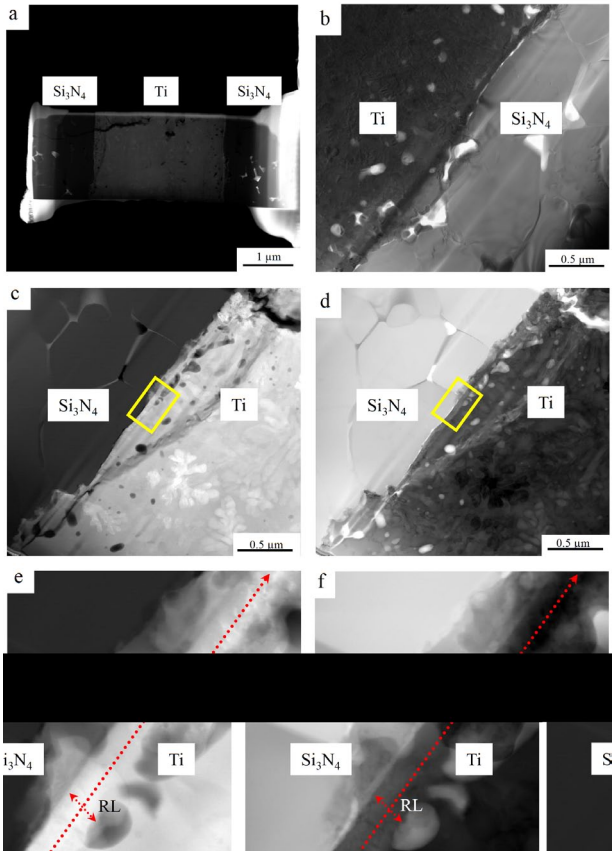

Fig. 2 (a, c, e) STEM–HAADF images of HT and FIBed Si_3N_4–Ti sample, (b) zero loss images of FIBed Si_3N_4–Ti joints, and (d, f) BF images of Si_3N_4–Ti joints.

diffraction contributions of equal phases (Figs. 2(d)–2(f)). Thus, new phase formations were detected by using unique contrast mechanism techniques.

To explore the chemical contents of resulting phases after heat-treatment, energy filtering and EELS-based SI analyses were carried out (Figs. 3–7). Due to the fact that joining and heat-treatment processes were conducted in air atmospheric conditions, Si_3N_4–Ti systems were comprised of just Si, N, and Ti elements, the major EELS $L_{2,3}$ (Si: 99 eV and Ti: 456 eV) and K (N: 401 eV and O: 532 eV) edges were used to view the corresponding elements in EFTEM 3-window analysis (Figs. 3(a)–3(d)). Considering the EFTEM maps, Si and N diffusion towards Ti foil side was detected. Here, effect of heat treatment on the enhancing of diffusion rate in both Si and N elements was obviously seen when compared to our former research [25]. Similar to TEM and STEM images (Fig. 2), the new dendritic phases can be also chemically observed in EFTEM maps (Figs. 3(a)–3(d)). From these maps, it was concluded that N and Si elements appeared in the chemical compositions of these newly

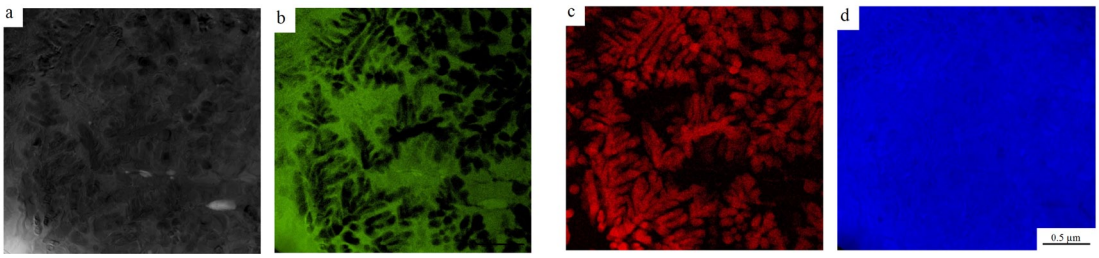

Fig. 3 (a) Zero loss image (20 eV), (b) Si–$L_{2,3}$, (c) N–K, and (d) Ti–$L_{2,3}$ EFTEM 3-window element maps showing different phase occurrence at HT Si_3N_4–Ti interface.

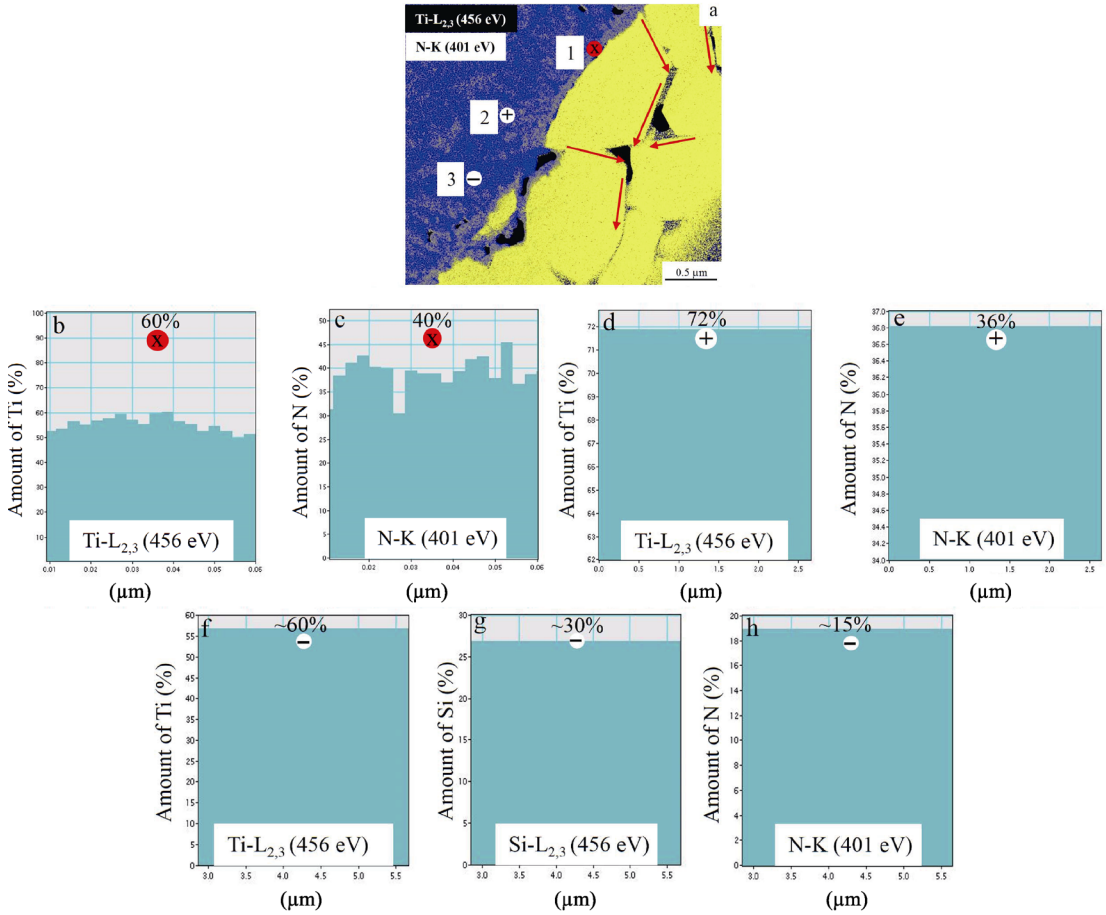

Fig. 4 (a) EFTEM–SI spectrum image (50–650 eV), (b, c) atomic quantity of Ti and N from point 1 (marked with red), (d, e) atomic quantity of Ti and N from point 2 (marked with green), and (f–h) atomic quantity of Ti, Si, and N from point 3 (marked with yellow) in (a).

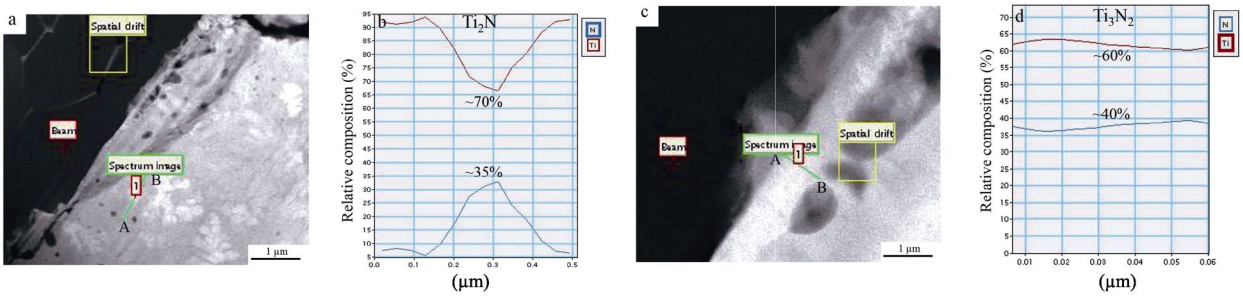

Fig. 5 (a, c) STEM–HAADF quantitative mapping for heat treated Si_3N_4–Ti sample, (b) Ti/N relative composition given by quantitative line analysis along the green line between A and B corresponding to Ti_2N phase, and (d) Ti/N relative composition given by quantitative line analysis along the green line between A and B corresponding to Ti_3N_2 phase.

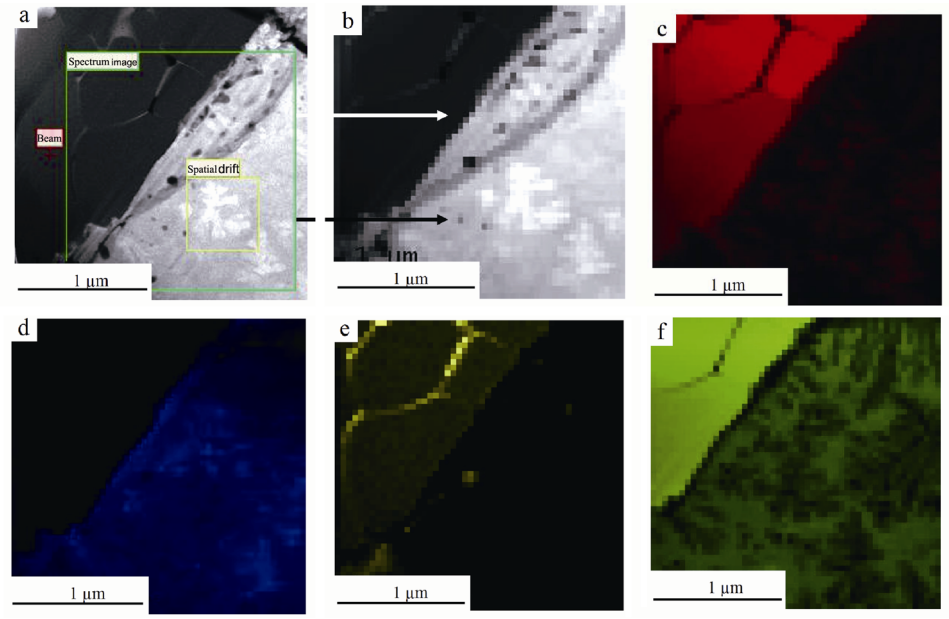

Fig. 6 (a) STEM–HAADF image showing where spectrum image area was acquired from (b) spectrum image; STEM–SI–EELS elemental mapping of (c) Si–$L_{2,3}$, (d) Ti–$L_{3,2}$, (e) O–K, and (f) N–K edges.

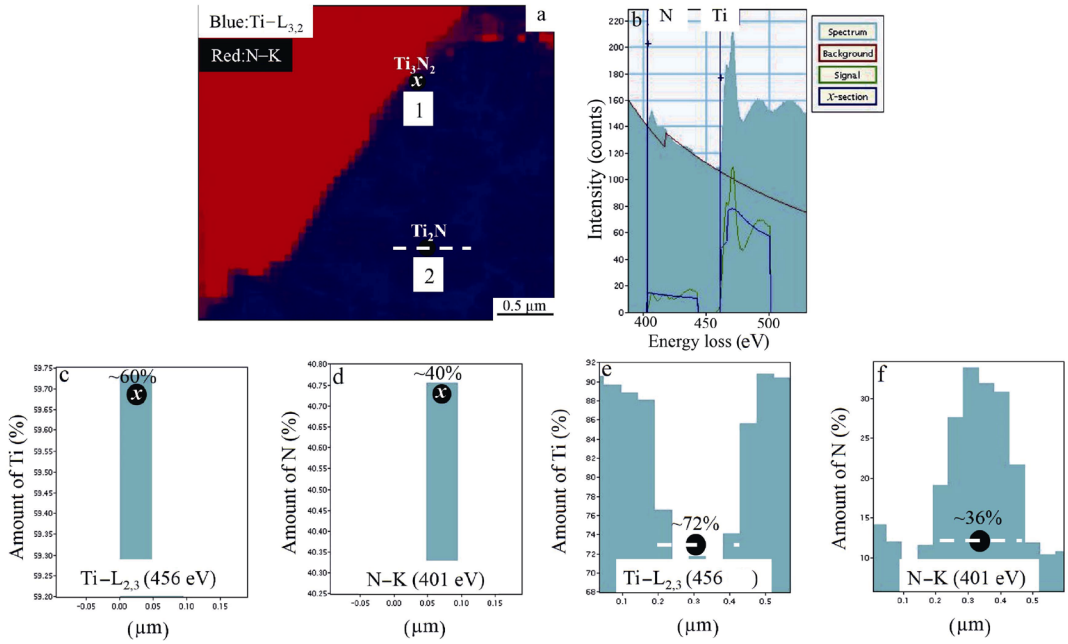

Fig. 7 (a) STEM–SI spectrum image, (b) STEM–SI–EELS quantitative elemental line scan spectrum obtained by N–K and Ti–$L_{2,3}$ edges along the dashed white line, (c, d) atomic quantity of Ti and N from point 1 corresponding to Ti_3N_2 phase (marked with black), and (e, f) atomic quantity of Ti and N from point 2 along to dashed line corresponding to Ti_2N phase (marked with black).

formed phases, but their stoichiometry of these phases can be generally considered as Ti_xN_y and Ti_xSi_y. Figure 3(c) shows the N distribution in the Ti interlayer as a dendritic form, while Si was distributed around this dendritic phase in the rest of the interlayer.

To further identify and quantify the phase content of occurred phases within the ceramic–metal joint material by CDJ method following the heat-treatment, SI analysis in EFTEM mode was conducted (Fig. 4). Herein, parallel energy planes in the 50–650 eV range were firstly acquired to construct the EFTEM–SI data cube including major $L_{2,3}$ and K edges of Si, Ti, and N

elements. Then, quantitative maps from the Si–$L_{2,3}$, N–K, and Ti–$L_{2,3}$ edges in SI data cube were extracted. Furthermore, the precise chemical composition of any desired region on the SI image can be quantitatively calculated. For new phase formations here, the atomic percentages for Ti and N elements in the intentionally selected points 1 and 2 (red and white, respectively) were determined and given in Figs. 4(b)–4(e). Based on the data (Figs. 4(b)–4(e)), the chemical contents of 1 and 2 points in at% were calculated as 60Ti–40N and 72Ti–36N, respectively. These findings reveal that the RL (point 1) was in Ti_3N_2 composition while the dendritically occurred phases in Ti foil side (point 2) were in Ti_2N composition. This phase (Ti_2N) was also observed in previous studies; however, there was no data in terms of the morphology of the phase [29–31] exception of Lenguaer's report [19], which expressed that Ti_2N phase was clearly formed by an acicular form. Furthermore, the chemical composition of 3 point (marked with white color) in at% was calculated as 60Ti–30Si–15N (Figs. 4(f)–4(h)). These results show that dendritic Ti_2N phases were surrounded by Ti_6Si_3N phases. More interestingly, we found that Ti diffused by interlayer to Si_3N_4 ceramic side by means of grain boundaries (marked with red arrows in Fig. 4(a)).

To confirm the obtained quantitative SI analyses results that acquired in EFTEM mode (Fig. 4), advance similar SI analyses in STEM mode were also carried out in Figs. 5–7. First line scan EELS analysis extracted from STEM–SI data exhibited that dendritic-shape phase was Ti_2N by averaging the data (70Ti–30N, at%) and the RL with around 50 nm thickness was Ti_3N_2 (60Ti–40N, at%) across the green-line between A and B points (Fig. 5). At this point, we point out that Ti interlayer accepted to Si and N elements by diffusion route to be formed the dendritic-shape Ti_2N phases. Moreover, Ti_2N was enclosed by Si rich as well as N bearing $Ti_{60}Si_{30}N_{15}$ phase (approximately Ti_6Si_3N).

Figures 6 and 7 show the EELS elemental maps and EELS quantitative line scan analyses extracted from the SI data cube that acquired in STEM mode, respectively. The atomic percentages of Ti and N were quantitatively determined by interaction and RL phases. Here, the chemical composition of point 1 (showed with black color) in at% was identified as 60Ti–40N (Figs. 7(c) and 7(d)) corresponding to Ti_3N_2 interaction phase, and white-dashed line marked with point 2 was 72Ti–36N (Figs. 7(e) and 7(f)), which equals to Ti_2N composition for RL phase. Therefore, we clearly state that these EELS results obtained by SI data in STEM mode support their counterparts acquired in EFTEM mode (Fig. 4). Please note that possible Ti_6Si_3N phase cannot be counted by SI analysis in STEM mode owing to high intense nano-size converged electron probe in low-loss EELS region.

4 Discussion

Due to the fact that Ti shows high affinity for both N and Si as an active element, it is generally considered as main nitride and silicate former constituent. Thus, it is likely to form new phases such as Ti_xN_y and Ti_xSi_y for Si_3N_4–Ti system. Figures 6(c)–6(f) indicate the EELS maps extracted from SI data cube in mode for Si–$L_{2,3}$, Ti–$L_{2,3}$, O–K, and N–K energy losses, respectively. Recalling these results, elemental diffusion between Si_3N_4 and Ti is clearly visible for both sides of the joint. For instance, N and Si diffusion were detected in the whole Ti interlayer; meanwhile, Ti diffusion towards the ceramic side was determined. Prominently, O_2 was also concentrated at grain boundaries of Si_3N_4.

In general, there seems to be some evidence to indicate that diffusion rate was increased as a result of heat treatment, so possible phases were formed by severe chemical interaction at the interface and whole interlayer. Therefore, phase sequence of the system can be predictable according to Gibbs free energy values, activation, and ionization energy of the elements.

Principally, several chemical reactions can take place when Si_3N_4 and Ti foils are joined:

$$Si_3N_4 + Ti = Ti_xN_y + Si_{(s)} \quad (1)$$

$$Si + Ti = Ti_xSi_y \quad (2)$$

$$Si_3N_4 + Ti = Ti_xSi_yN_z \quad (3)$$

According to Refs. [18,29,31–33], even though Ti_2N and Ti_5Si_3N phases were reported by a number of researchers, the thermodynamics of these phases were not well-documented. Nevertheless, Ma *et al*. [21] and Sambasivan and Petuskey [23] reported Gibbs free energies of Ti–Si–N. In addition, the phase equilibrium systems of Ti–Si, Si–N, and Ti–N were studied [21,23,34,35]. These studies express that the formation of reactions among Ti, Si, and N can be given as following Eqs. (4)–(12) [18,36,37]:

$$1/9Si_3N_4 + Ti = 4/9TiN + 1/9Ti_5Si_3$$
$$\Delta G^\circ_{1400\,℃} = -140\ \text{kJ/mol [18]} \quad (4)$$
$$1/5Si_3N_4 + Ti = 1/5Ti_5Si_3(s) + 2/5N_{2(g)}$$

$$\Delta G^{\circ}_{1044\,℃} = -56.19\ \text{kJ [36]} \quad (5)$$

$$1/9Si_3N_4 + Ti = 4/9TiN + 1/9Ti_5Si_3$$

$$\Delta G^{\circ}_{1044\,℃} = -126.15\ \text{kJ [36]} \quad (6)$$

$$1/4Si_3N_4 + Ti = TiN + 3/4Si$$

$$\Delta G^{\circ}_{1044\,℃} = -136.46\ \text{kJ [36]} \quad (7)$$

$$2/3Si_3N_4 + Ti = TiSi_2 + 4/3N_2$$

$$\Delta G^{\circ}_{1044\,℃} = +43.56\ \text{kJ [36]} \quad (8)$$

$$Ti + 2Si = TiSi_2$$

$$\Delta G^{\circ}_{1044\,℃} = -162.13\ \text{kJ [36]} \quad (9)$$

$$Ti + 1/9Si_3N_4 = 4/9TiN + 1/9Ti_5Si_3$$

$$\Delta G^{\circ}_{1100\,℃} = -127.49\ \text{kJ/mol [37]} \quad (10)$$

$$Ti + 1/5Si_3N_4 = 1/5Ti_5Si_3 + 2/5N_{2(g)}$$

$$\Delta G^{\circ}_{1100\,℃} = -62.75\ \text{kJ/mol [37]} \quad (11)$$

$$Ti + 1/4Si_3N_4 = TiN + 3/4Si$$

$$\Delta G^{\circ}_{1100\,℃} = -135.39\ \text{kJ/mol [37]} \quad (12)$$

In addition, the driving force of Ti_2N and Ti_5Si_3N was reported by Ma *et al*. [21] as –0.681 and –0.0421 J/mol at 1100 ℃, respectively. On the other hand, Gibbs free energy of Ti_5Si_3 was given by ΔG^{o}= –194, 140+ 16.74T (J/mol) (T is the temperature) [37]. These results show that Ti_2N, Ti_5Si_3, and Ti_5Si_3N phase formations were possible. According to Singh *et al.* [36], $TiSi_2$ (Eq. (8)) formation was not possible, because Gibbs free energy was positive ($\Delta G^{\circ}_{1400\,℃}$ = +43.56 kJ), even though free energy of $TiSi_2$ (Eq. (9)) was negative ($\Delta G^{\circ}_{1400\,℃}$ = –162.13 kJ), it was still not expected to occur due to the lack of Si (Eq. (8)). Conversely, for reactions (4–6,10,11), Ti_5Si_3 phase formation was most favorable because of the negative value of free energy of formation, respectively ($\Delta G^{\circ}_{1400\,℃}$ = –140 kJ/mol, $\Delta G^{\circ}_{1400\,℃}$ = –56.19 kJ, $\Delta G^{\circ}_{1400\,℃}$ = –126.15 kJ, $\Delta G^{\circ}_{1400\,℃}$ = –127.49 kJ/mol, and $\Delta G^{\circ}_{1100\,℃}$ = −62.75 kJ/mol). On the other hand, TiN formation was likely to be occurred since ΔG^{o} was negative for reactions (4,6,7,10,12) [18,36,37]. Regarding Ti_5Si_3 and TiN, reaction (Eq. (4)) was more favorable than others as Huang *et al*. [18] were reported. Liu *et al*. [38] stated similar results for brazing ceramic using with Cu–Pd–Ti foil at 1150 ℃. The RL in TiN composition was formed. It is because lower free energy formation for TiN was –407.2 kJ/mol than that of Si_3N_4 and Ti_5Si_3, which were –137.8 and –173 kJ/mol, respectively. On the other hand, Zhang *et al*. [39] reported that the Gibbs free energies of TiN and Ti_5Si_3 at 950 ℃ were –564 and –173 kJ/mol, respectively. Furthermore, Shimoo *et al*. [40] investigated the Ti–N system under nitrogen and argon atmosphere, and they found that TiN and Ti_2N phases occurred below 800 ℃, whereas TiN, Ti_2N, and Ti_5Si_3 phases were observed below 1050 ℃.

Similar to our former research [25], after heat treatment at 1000 ℃, we also observed nearly uniform phase structures like performed previous studies [18, 19,36–40]. However, it can be explained that primary microstructure was consisted of Ti_3N_2 reaction layer with 50 nm thickness at the interface, dendritic shape Ti_2N phase instead of Ti_3N formation along the whole Ti interlayer and Si rich Ti_xSi_yN phases. Now, what we know about the formation of Ti_2N from Ti_3N is clearly based on the heat effect. Nevertheless, there is still no clear explanation on the fact that why change of round-shaped morphology of Ti_3N phase to dendritic Ti_2N phase took place during the heat treatment. On the other hand, as a result of decomposition of Si_3N_4, Si and N atoms diffused towards the interlayer and reacted with Ti interlayer. However, N atoms might be raised due to the furnace conditions. It was because that heat treatment was performed in air at 1000 ℃.

In principle, there are several possible diffusion paths or reaction mechanism:

Firstly, it was stated that composition and Ti_3N_2 reaction layer thickness evolved in interface did not change after heat treatment. This means that observed reaction layer was stable at around 1000 ℃. This can also be explained by the passing of high-energy pulse through the interlayer which may increase the temperature around the melting point of Ti, thus the active liquid Ti and N react rapidly at the ceramic interface [22]. In addition, since joining is completed in micro seconds, very thin Ti_3N_2 reaction layer might be attributed to this very short process time. As can be clearly seen according to Figs. 2(c)–2(e), liquid Ti attacked to the ceramic side to form Ti_3N_2 reaction layer and free Si (Eq. (13)). Lemus *et al*. [14] argued that the interface phase was TiN between Si_3N_4 and Ti, but Maeda *et al*. [13] suggested that the observed phase was Ti_5Si_3 rather than Ti_xN_y. However, as a result of Ti_3N phase transformation to Ti_2N (Eq. (14)) phase under the heat effect, released free Ti and Si atoms would react and form Ti_6Si_3N phases which are isolating the dentritic shape Ti_2N phases. Sambasivan and Petuskey [23] reported that with increasing N activity, α-Ti altered to β-Ti which transforms the Ti_2N to TiN_x. Ti_3N_2 reaction layer that formed earlier acts as

a barrier to block further reactions between Si_3N_4 and Ti interlayers. Under these circumstances, it is assumed that first free Si atoms diffused towards Ti interlayer as a result of rapid decomposition of Si_3N_4 to form Ti_6Si_3N phases since the activation energy for the diffusion of Si in Ti was faster than N in Ti [14]. Thus, Si atoms were reacted with Ti at the interlayer, and then Ti_2N was formed and isolated by new Ti_5Si_3N phases. This fact indicates that Ti_3N_2/Ti_6Si_3N–Ti_2N phase sequence is expected to occur in this condition. Ref. [21] indicating that N solubility in Ti_5Si_3 was 11 at%, it is most likely that formation of Ti_6Si_3N phase could occur since driving force for this reaction and/or diffusion was very low [20]. After, Ti_6Si_3N phase reaches to stable state, the Ti_3N_2 reaction layer possibly occurs after the reaction between Ti and N. Alternatively but less likely, Ti_5Si_3/Ti_6Si_3N–Ti_3N_2 phase sequence can occur. Conversely, Lengauer *et al*. [41] reported that isothermal diffusion couple with the phase sequence was Ti(N)/Ti_3N_{2-x}/Ti_2N/TiN_{y-x} for Ti–N systems.

Another but less likely possibility is Ti_2N phase that may be generated by Ti_3N_2 phase dissociation (Eqs. (15) and (16)) or reaction between the Ti_3N_2 and Ti in the Ti metal foil side of the joint (Eq. (17)). Additionally, Ti_6Si_3N phase evolution may be achieved by the possible reaction taking place between the Ti_2N and Si constituents (Eq. (18)).

Therefore, below reactions for the development of related phases can be proposed:

$$6Ti + Si_3N_4 \rightarrow 2Ti_3N_2 + 3Si \quad (13)$$

$$Ti_3N \rightarrow Ti_2N + Ti \quad (14)$$

$$3Ti_3N_2 + 3Si \rightarrow Ti_5Si_3 + 2Ti_2N + 2N_{2(g)} \quad (15)$$

$$Ti_3N_2 \rightarrow Ti_2N + Ti + 1/2N_{2(g)} \quad (16)$$

$$3Ti_3N_2 + Ti \rightarrow 5Ti_2N + 1/2N_{2(g)} \quad (17)$$

$$3Ti_2N + 3Si \rightarrow Ti_6Si_3N + 1/2N_{2(g)} \quad (18)$$

It is important to state that Ti_6Si_3N, Ti_3N_2, and Ti_2N phases have not been so far visualized by using advanced and analytical TEM techniques at heat-treated Si_3N_4–Ti interfaces, until current research are performed. Although their formations were known in Refs. [33,41], but only limited thermodynamically discussion for these reactions were available. Therefore, it is thought that our detailed TEM data presented herein will pave a new way to combine the thermodynamic approach and analytical imaging techniques.

5 Conclusions

A heat treatment process on a ceramic–metal joint material consisted of Si_3N_4–Ti phases through CDJ method was applied in air atmosphere at 1000℃. Electron transparent samples from heat-treated Si_3N_4–Ti ceramic–metal joint material for advanced TEM-based analysis, e.g., SI, EFTEM, EELS, and STEM, were prepared by FIB method. Based on the detailed TEM results, Si and N diffusion arising from the Si_3N_4 ceramic was observed towards Ti metal foil side and further interacted with Ti atoms. Ti_3N_2 reaction layer with 50 nm thickness were formed at the interface while Ti_6Si_3N matrix phase including dendritic-shaped Ti_2N grains occurred in the Ti interlayer. It is believed that our TEM-based microscopy results not only provide the knowledge on ceramic–metal joint materials by CDJ method, but also contribute new insights on the development of various new joint systems.

Acknowledgements

The authors would like to thank to Anadolu University (Eskisehir, Turkey) for financial support by BAP-030217 project. We would like to also give our gratitude to UNAM Laboratories of Bilkent University (Ankara, Turkey) for FIB analysis.

References

[1] Riley FL. Silicon nitride and related materials. *J Am Ceram Soc* 2004, **83**: 245–265.
[2] Bocanegra-Bernal MH, Matovic B. Mechanical properties of silicon nitride-based ceramics and its use in structural applications at high temperatures. *Mater Sci Eng* 2010, **527**: 1314–1338.
[3] Zheng GM, Zhao J, Gao ZJ, *et al*. Cutting performance and wear mechanisms of SiAlON–Si_3N_4 graded nano-composite ceramic cutting tools. *Int J Adv Manuf Technol* 2012, **58**: 19–28.
[4] Veiga C, Davim JP, Loureiro AJR. Properties and applications of titanium alloys: a brief review. *Rev Adv Mater Sci* 2012, **32**: 133–148.
[5] Myers JR, Bomberger HB, Froes FH. Corrosion behavior and use of titanium and its alloys. *JOM* 1984, **36**: 50–60.
[6] Chuvil'Deev VN, Kopylov VI, Nokhrin AV, *et al*. Study of mechanical properties and corrosive resistance of ultrafine-grained α-titanium alloy Ti-5Al-2V. *J Alloys Compd* 2017, **723**: 354–367.
[7] Martinsen K, Hu SJ, Carlson BE. Joining of dissimilar materials. *Cirp Ann* 2015, **64**: 679–699.
[8] Schwartz MM. *Handbook of Structural Ceramics*. New

York: McGraw-Hill Press, 1992.
[9] Groche P, Wohletz S, Brenneis M, *et al*. Joining by forming—A review on joint mechanisms, applications and future trends. *J Mater Process Technol* 2014, **214**: 1972–1994.
[10] Morales-Pérez M, Ceja-Cárdenas L. Interfacial characterization in the brazing of silicon nitride to niobium joining using a double interlayer. *Mater Charact* 2017, **131**: 316–323.
[11] Asthana R, Singh M, Martinez-Fernandez J. Joining and interface characterization of *in situ* reinforced silicon nitride. *J Alloys Compd* 2013, **552**: 137–145.
[12] Fernie JA, Drew RAL, Knowles KM. Joining of engineering ceramics. *Int Mater Rev* 2009, **54**: 283–331.
[13] Maeda M, Oomoto R, Shibayanagi T, *et al*. Solid-state diffusion bonding of silicon nitride using titanium foils. *Metall and Mat Trans A* 2003, **34**: 1647–1656.
[14] Lemus J, Drew RAL. Joining of silicon nitride with a titanium foil interlayer. *Mater Sci Eng* 2003, **352**: 169–178.
[15] Koleňák R, Kostolný I, Kusý M. Characterization of soldering alloy type Zn-In-Mg and the study of direct soldering of silicon and copper. *Mater Sci Eng* 2018, **712**: 302–312.
[16] Kolenak R. Study of direct soldering of silicon and copper substrate by use of Bi-based solders with lanthanides addition. *Solder Surf Mo Technol* 2017, **29**: 121–132.
[17] Koleňák R, Kostolný I, Drápala J, *et al*. Characterizing the soldering alloy type In–Ag–Ti and the study of direct soldering of SiC ceramics and copper. *Metals* 2018, **8**: 274–290.
[18] Huang QL, Cai J, Pan W, *et al*. *In situ* processing of TiN/Si_3N_4 composites by $Ti\text{-}Si_3N_4$ solid state reaction. *Mater Lett* 1997, **31**: 221–225.
[19] Lengauer W. A study of δ′-TiN_{1-x} formation in temperature gradient diffusion couples. *J Alloys Compd* 1992, **179**: 289–297.
[20] Paulasto M, Kivilahti JK. Formation of interfacial microstructure in brazing of Si_3N_4 with Ti-activated Ag-Cu filler alloys. *Scr Metall Et Mater* 1995, **32**: 1209–1214.
[21] Ma XY, Li CR, Zhang WJ. The thermodynamic assessment of the Ti–Si–N system and the interfacial reaction analysis. *J Alloys Compd* 2005, **394**: 138–147.
[22] Zhang RF, Veprek S. On the spinodal nature of the phase segregation and formation of stable nanostructure in the Ti–Si–N system. *Mater Sci Eng* 2006, **424**: 128–137.
[23] Sambasivan S, Petuskey WT. Phase chemistry in the Ti-Si-N system: Thermochemical review with phase stability diagrams. *J Mater Res* 1994, **9**: 2362–2369.
[24] Turan S, Bucklow IA, Wallach ER. Capacitor-discharge joining of oxide ceramics. *J Am Ceram Soc* 2004, **82**: 1242–1248.
[25] Tunckan O, Yurdakul H, Turan S. Identification and quantification of reaction phases at Si_3N_4–Ti interfaces by using analytical transmission electron microscopy techniques. *Ceram Int* 2013, **39**: 1087–1095.
[26] Turan S, Turan D, Bucklow IA, *et al*. Microstructure of capacitor discharge joined SiAlON and silicon nitride ceramics. *Inst Phys Conf* 2001, **168**: 319–322.
[27] Takaki K, Takada Y, Itagaki M, *et al*. Bonding strength of alumina tiles joined using capacitor discharge technique. *Surf Coat Technol* 2003, **169–170**: 495–498.
[28] Tunçkan O, Turan D, Doğan A, *et al*. Characterization of the interfaces formed at the silicon nitride superalloy joints. *J Aust Ceram Soc* 2017, **53**: 83–89.
[29] Yang RK, Zhu CS, Wei Q, *et al*. Investigations on structural, elastic, thermodynamic and electronic properties of TiN, Ti_2N and Ti_3N_2 under high pressure by first-principles. *J Phys Chem Solids* 2016, **98**: 10–19.
[30] Farè S, Lecis N, Vedani M, *et al*. Properties of nitrided layers formed during plasma nitriding of commercially pure Ti and Ti–6Al–4V alloy. *Surf Coat Technol* 2012, **206**: 2287–2292.
[31] Yu HJ, Sun FJ. A modified embedded atom method interatomic potential for the Ti–N system. *Phys B Condens Matter* 2009, **404**: 1692–1694.
[32] Wang TP, Liu CF, Leinenbach C, *et al*. Microstructure and strengthening mechanism of Si_3N_4/Invar joint brazed with TiNp-doped filler. *Mater Sci Eng* 2016, **650**: 469–477.
[33] Mishra SC, Nayak BB, Mohanty BC, *et al*. Surface nitriding of titanium in arc plasma. *J Mater Process Technol* 2003, **132**: 143–148.
[34] Yang JY, Wu JS, Hua W. Study on mechanical alloying and subsequent heat treatment of the Ti–Si system. *Phys B Condens Matter* 2000, **279**: 241–245.
[35] Wriedt HA, Murray JL. The N-Ti (nitrogen-titanium) system. *Bull Alloy Phase Diagrams* 1987, **8**: 378–388.
[36] Singh M, Asthana R, Varela FM, *et al*. Microstructural and mechanical evaluation of a Cu-based active braze alloy to join silicon nitride ceramics. *J Eur Ceram Soc* 2011, **31**: 1309–1316.
[37] Wei P, Chen J, Huang Y. Titanium metallization of Si_3N_4 ceramics by molten salt reaction: Mechanism and interfacial structure. *J Mater Sci* 2000, **35**: 3685–3689.
[38] Liu CF, Zhang J, Zhou Y, *et al*. Effect of holding time on the self-joining of silicon nitride. *J Alloys Compd* 2009, **471**: 217–221.
[39] Zhang J, Zhang XM, Zhou Y, *et al*. Interfacial microstructure of Si_3N_4/Si_3N_4 brazing joint with Cu–Zn–Ti filler alloy. *Mater Sci Eng* 2008, **495**: 271–275.
[40] Shimoo T, Okamura K, Adachi S. Interaction of Si_3N_4 with titanium at elevated temperatures. *J Mater Sci* 1997, **32**: 3031–3036.
[41] Lengauer W, Bauer J, Guillou A, *et al*. WDS-EPMA Nitrogen profile determination in TiN/Ti diffusion couples using homotypic standard materials. *Mikrochim Acta* 1992, **107**: 303–310.